




Liquid-phase exfoliation of WSe₂ nanosheets for ITO/WSe₂ photodetector

Badal L. Chauhan^{1,*} , Sanjay A. Bhakhar¹, Pratik M. Pataniya², Shubham U. Gupta¹, G. K. Solanki^{1,*}, V. M. Pathak¹, and Vikas Patel³

¹Department of Physics, Sardar Patel University, Vallabh Vidyanagar, Anand 388120, Gujarat, India

²Department of Physical Science, P.D. Patel Institute of Applied Sciences, Charorat University of Science and Technology, CHARUSAT, Changa, Gujarat 388421, India

³Sophisticated Instruments Centre for Applied Research and Testing-SICART, Vallabh Vidyanagar, Gujarat 388120, India

Received: 1 February 2022

Accepted: 28 February 2022

Published online:
15 March 2022

© The Author(s), under exclusive licence to Springer Science+Business Media, LLC, part of Springer Nature 2022

ABSTRACT

The potential application of atomically thin two-dimensional (2D)-layered WSe₂ in future wearable electronics has sparked a lot of interest. Herein, we report the highly crystalline nature of WSe₂ nanosheets was synthesized by the liquid-phase exfoliation technique and its application as a broadband photodetector. The direct vapor transport (DVT) technique has been used in the synthesis of bulk WSe₂ compounds. The chemical composition and purity of the grown compound were investigated by EDAX (Energy-dispersive analysis of X-ray). The structural phase analysis and the crystalline orientation were examined by X-ray diffraction technique (XRD), Scanning electron microscopy (SEM), and High-resolution transmission electron microscopy (HR-TEM) of the synthesized WSe₂ compound. The Raman spectrum depicts the resonances corresponding to the E_{2g} mode of vibration of WSe₂ nanosheets. Additionally, a broadband photodetector based on WSe₂ nanosheets was constructed and evaluated under wavelength-dependent illumination sources with a power level of 40 mW/cm² on a 1.0 bias voltage. The ITO/WSe₂ nanosheet device was studied under the function of various power intensities and various external bias voltages. The device is tested for bias between 0 and 30 V and its responsiveness is improved. Furthermore, the device demonstrated higher stability under 40 mW/cm² intensity. The results showed that WSe₂ nanosheets have good optoelectronic capabilities and can be used in future optoelectronic devices.

Address correspondence to E-mail: b.chauhan389@gmail.com; solankigunvant@yahoo.co.in

1 Introduction

The advent and progress in the field of layered semiconducting 2D materials with substantial optoelectronic capabilities in recent years have sparked interest in finding new ways to fabricate electrical and optoelectronic devices using these atomically thin layers. [1, 2]. This situation prompted extensive research interest in 2D materials such as phosphorene [3], BN [4, 5], TMDCs [6–11], and TMTCs [12–15]. Bulk TMDCs materials having a 2-H phase behave as an indirect bandgap semiconductor. When their thickness is reduced to monolayer, they behave like direct bandgap semiconductors [16]. MX_2 is a general chemical formula for layered 2D materials containing M as transition metal (e.g., titanium (Ti), niobium (Nb), nickel (Ni), tantalum (Ta), molybdenum (Mo), and tungsten(W)) and X as chalcogen atoms (e.g., sulfur(S), selenium (Se), and tellurium (Te)). TMDCs have layers of transition metal sandwiched between two chalcogen atoms with strong in-plane covalent bonds between the transition metal and chalcogen atoms in their crystalline structure. On the other side, the weak van der Waals type interaction exists between MX_2 layers [17–21]. Tungsten diselenide (WSe_2), a member of the TMDCs family, has been successfully used for a variety of potential applications, including optoelectronic devices, solar cells, field-effect transistors (FETs), and various photodetectors.

The tungsten diselenide is formed as an atomically small-dimensional layer by sandwiching a W-atom layer between two Se-atom layers via covalent bonds in a crystallographic c-axis with a Se–W–Se layer structure. The bulk WSe_2 crystal is formed of WSe_2 tri-layers stacked together by weak van der Waals interaction and then causes exfoliation into a single isolated layer using various exfoliation techniques, such as mechanical, chemical, liquid phase, and electrochemical exfoliation are available [22–24]. Among these methods, liquid-phase exfoliation (LPE) is widely used because solvents like acetone, water, and NMP (N-Methyl-2-pyrrolidone) are easily accessible [25–27]. In this article, we presented the liquid-phase exfoliation of WSe_2 nanosheets and the fabrication of a photodetector from WSe_2 nanosheets. The photodetector parameters like specific detectivity, photoresponsivity, and response time are measured. ITO/ WSe_2 nanosheets/ITO photodetector is a

non-ohmic and asymmetric contact-based device with fast photoswitching action.

2 Experimental details

2.1 Synthesis of pure WSe_2 nanosheets

The WSe_2 powder is grown by the direct vapor transport technique [28]. The Solution-phase exfoliation technique was used to synthesize good-quality WSe_2 nanosheets. N-methyl-2-pyrrolidone was used as exfoliation medium due to suitable surface energy. For the exfoliation process, 50 mg bulk WSe_2 was grinded using mortar pestle. The crushed powder was dispersed in the 20 ml NMP and the prepared solution was sonicated in a bath sonicator for 12 h. The frequency of the ultrasound is 40 kHz and has 100-W power. The resulting yields were dark black in color after 12 h of sonication, and the shift in suspension color from shiny gray to dark black indicates that the WSe_2 was adequately disseminated in NMP and properly exfoliated. The centrifugation was carried out for sonicated suspension at 4500 rpm for 20 min. The suspension contains a few layers of WSe_2 nanosheets and unexfoliated sludge. The supernatant was retained for further study and characterization [29–33].

2.2 Characterization

The investigation of elemental purity and stoichiometry of bulk and exfoliated WSe_2 is done using energy-dispersive X-ray analysis (EDAX). The structural phase analysis of bulk and exfoliated WSe_2 was carried out by the Power X-ray diffraction technique (PXRD) using a Rigaku Ultima diffractometer having $\text{Cu}(k\alpha)$ radiation source (1.546 Å). The morphology and surface topology of bulk and exfoliated nanosheets of the WSe_2 were also studied using scanning electron microscopy (SEM). The High-resolution transmission electron microscopy (HR-TEM) and the selected area electron diffraction (SEAD) were used to examine the morphology and crystalline orientation of the exfoliated WSe_2 nanosheets. The vibrational modes of bulk and exfoliated WSe_2 were studied by Raman spectroscopy. Spectrophotometer was used to record the absorption spectrum of exfoliated WSe_2 nanosheets in the spectral region 400–1000 nm.

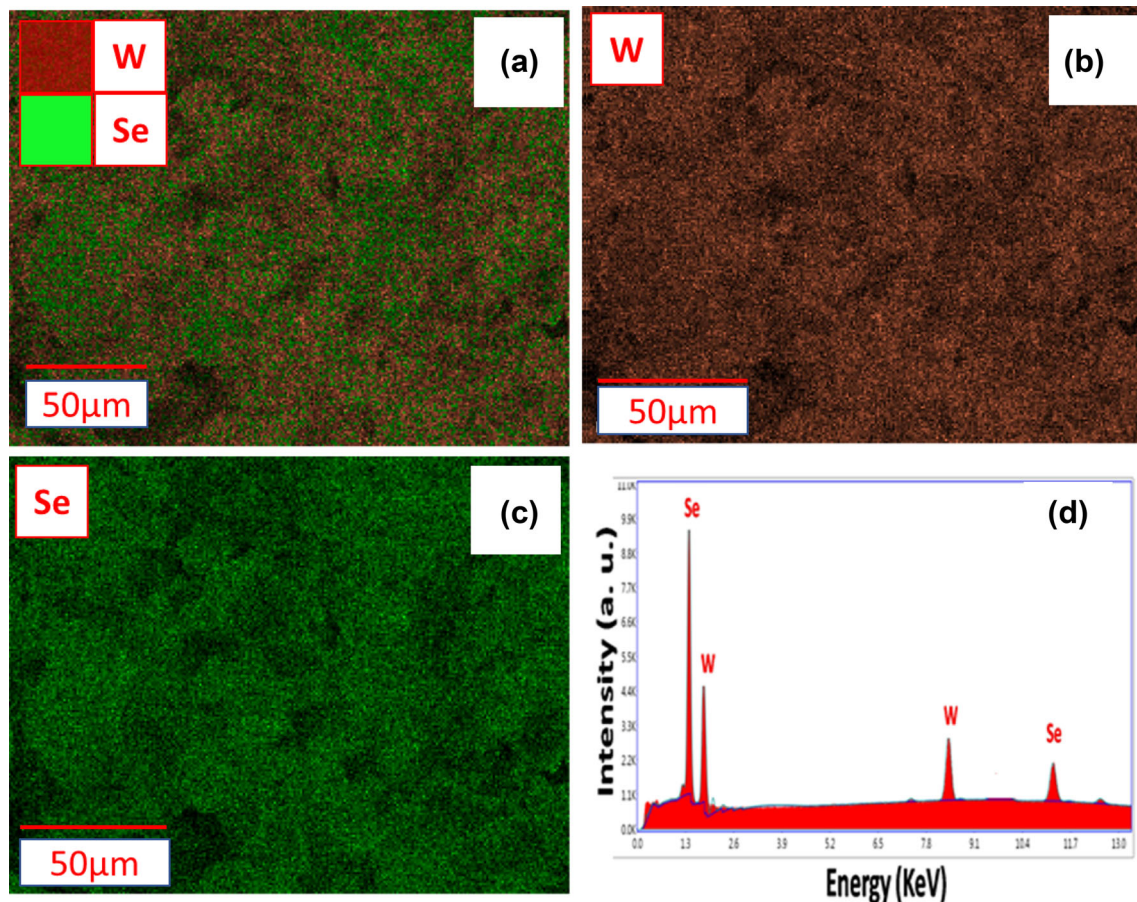


Fig. 1 a–c Elemental mapping. d Energy-Dispersive Analysis of X-ray spectrum of exfoliated nanosheets of WSe_2

2.3 Fabrication of photodetector

To fabricate the photodetector, the channel of length 1 mm was created by making a groove on the ITO-coated glass using a cutter. Then, the suspension of WSe_2 nanosheets was repeatedly drop-casted onto a channel region on preheated (60 °C) glass substrate. The NMP traces were completely removed by annealing for 2 h at 120 °C in a vacuum. Copper wire was bonded to the thin-film edge with conducting Ag paste to form ohmic connections. The fabricated device was fixed on the printed circuit board (PCB). Keithly-4200 SCS (semiconductor characterization system) was used to measure current–voltage characteristics in a bias range of ± 10.0 V in dark condition and in illuminated condition. We have also measured the wavelength-dependent photoresponse of the fabricated device under periodic illumination with monochromatic sources, such as blue (470 nm), green (540 nm), and red (670 nm), and polychromatic sources such as pink and white of 40 mW/cm² power

intensity at 1.0 bias voltage. The photodetector was exposed under 10-s periodic illumination of a polychromatic pink light source with power intensity ranging from 5 to 40 mW/cm² and an external bias of 0.5 to 5.0 V was set, followed by a pulse photodetection experiment.

3 Results and discussion

Firstly, the WSe_2 nanosheets were synthesized using the liquid-phase exfoliation technique (LPE). The chemical composition and purity were investigated by the elemental mapping and EDAX spectra. The elemental mapping of W and Se in WSe_2 nanosheets shown in Fig. 1a–c. The weight percentage of constituents (W) $\sim 54\%$ and (Se) $\sim 46\%$ from the EDAX and weight percentage taken for the growth are (W) $\sim 53.8\%$ and (Se) $\sim 46.2\%$ which are well matched. It was examined that the all elements are uniformly distributed. There are no extra peaks observed

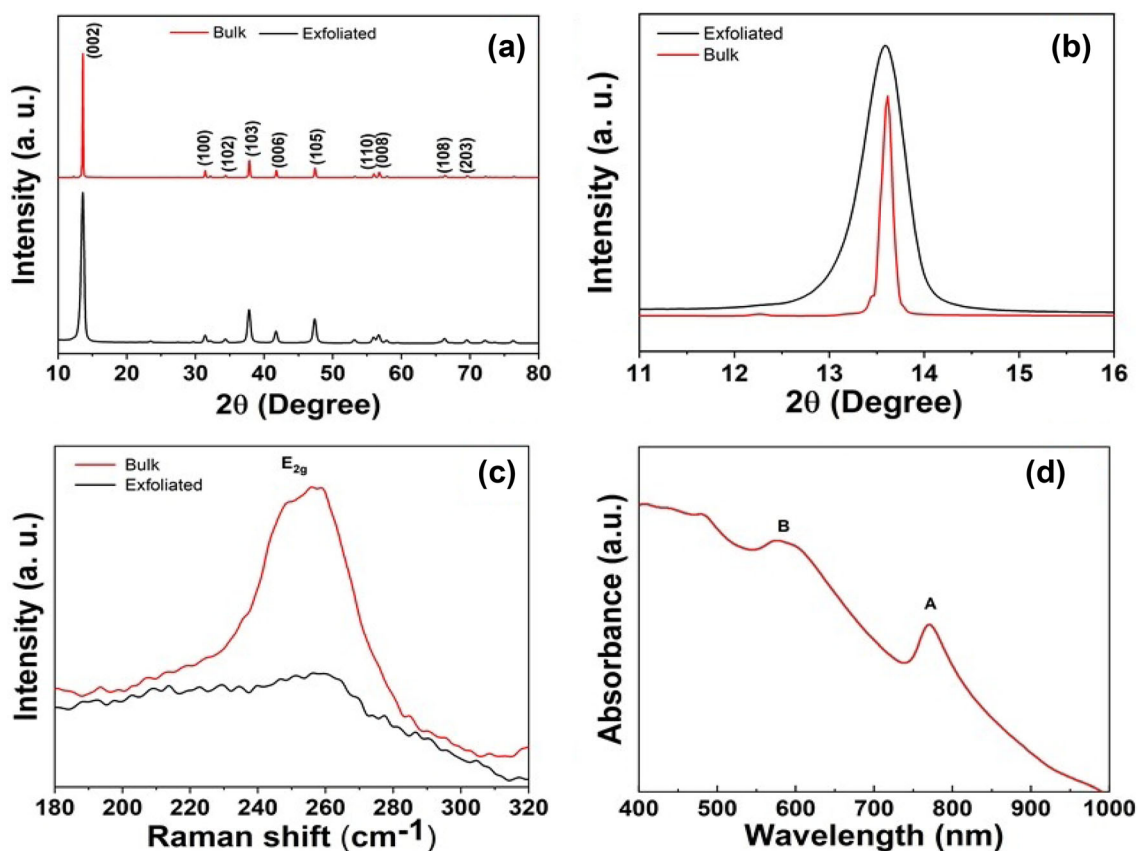


Fig. 2 a Powder XRD pattern. b Broadened view of (002) plane of WSe₂. c Raman spectrum of grown and exfoliated WSe₂. d Absorption spectrum

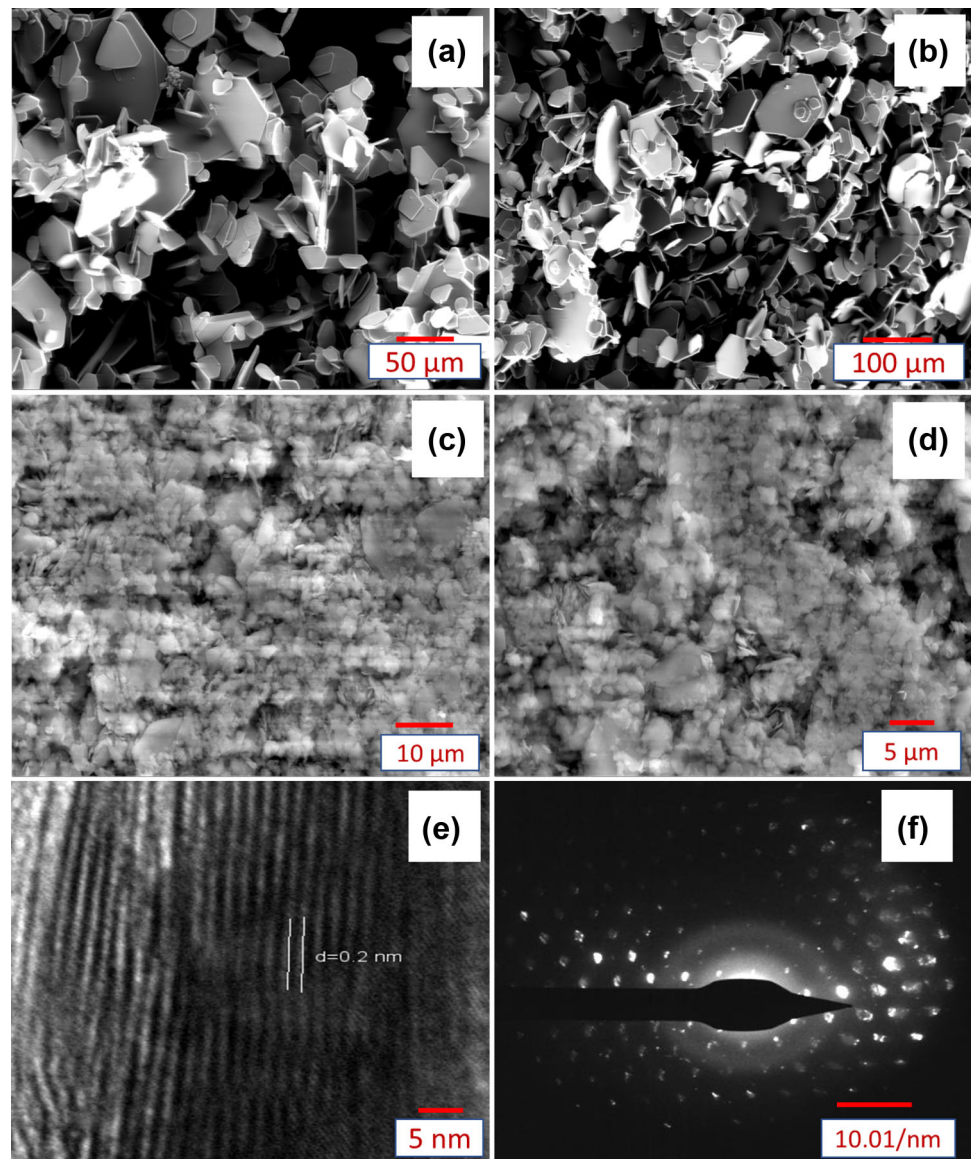
in EDAX spectra of WSe₂ nanosheets which confirm the chemical purity of the nanosheets that is shown in Fig. 1d.

The structure of bulk and exfoliated WSe₂ compound was investigated by the powder X-ray diffraction (PXRD) technique. Figure 2a represents the PXRD patterns of bulk and exfoliated WSe₂ material having hexagonal lattice structure. The lattice parameters, calculated from the PXRD pattern, are $a = b = 3.285 \text{ \AA}$ and $c = 12.976 \text{ \AA}$ which are well matched with reported values [25]. The lattice parameters of bulk and exfoliated WSe₂ are found to be almost similar. There are no secondary or impurity phase peaks found in the PXRD pattern, indicating that the synthesized materials have higher structural phase purity [34]. The presence of sharp PXRD peaks indicates the high crystallinity of WSe₂ nanosheets. Figure 2b represents the magnified image of (002) peak of bulk and exfoliated WSe₂. Broadening of the (002) peak shows the decrease in the crystallite size in exfoliated WSe₂ as compared with bulk WSe₂ [35, 36].

Raman spectroscopy is a key method for the investigation of vibrational modes. It has been proved to be a useful technique to determine layers in 2D-TMDs materials [35, 36]. Figure 2c shows the Raman spectrum of bulk and exfoliated WSe₂ compounds. In the Raman spectrum, an in-plane E_{2g} vibration mode is observed in both bulk as well as exfoliated WSe₂ compounds. The corresponding wavenumber of E_{2g} vibrational mode for bulk material is 255 cm^{-1} , whereas for exfoliated material, it is 256 cm^{-1} with less intensity. The shift in peak observed in Raman spectrum explains the exfoliation of a few layers of WSe₂ nanosheets. In this E_{2g} mode, tungsten and selenium atoms vibrate in the basal plane opposite to each other. Figure 2d indicates the absorption spectrum of WSe₂ nanosheets in the spectrum range of 400–1100 nm, and the A and B excitonic transitions are represented by two peaks at 770 and 579 nm, respectively [35, 37].

The SEM images of the as-grown bulk WSe₂ are shown in Fig. 3a and b having hexagonal morphology. The SEM images show the WSe₂ uniform

Fig. 3 a, b SEM images of grown WSe₂ compounds. c, d SEM image of exfoliated nanosheets of WSe₂. e HR-TEM image of WSe₂ Nanosheets. f SAED pattern of exfoliated WSe₂ nanosheets



distribution nanosheets of ITO-coated glass substrate which are shown in Fig. 3c and d. SEM images taken at various length scales reveal a continuous film with flakes of various lateral sizes. The morphological study of WSe₂ nanosheets was investigated by high-resolution transmission electron microscopy (HR-TEM). Figure 3e shows the HR-TEM image of WSe₂ nanosheets at 5-nm resolution. Moiré fringes show the interplanar distance of 0.20 nm for WSe₂ nanosheets. The inclusion of a distinct spot pattern in the SAED pattern in Fig. 3f indicates that the WSe₂ has a single crystallinity [35, 37].

Figure 4a depicts the schematic diagram of ITO/WSe₂ nanosheet-based photodetector. In addition, I-V studies and pulse photoresponse experiments were

carried out under illumination of different monochromatic and polychromatic wavelength sources of 40 mW/cm² power intensity for 1.0 V external bias. We used monochromatic sources, such as blue light (470 nm), green light (540 nm), and red light (670 nm), as well as polychromatic sources, such as white and pink light. The total current is significantly increased due to the contribution of photocurrent which is seen from Fig. 4b of source-dependent I-V characteristics. Figure 4c shows the 1.0 V external bias responses of the WSe₂-based photodetector versus periodic light pulses of sources for the source-dependent comparative analysis, in which observed rapid switching for all wavelength-dependent light sources proved that the

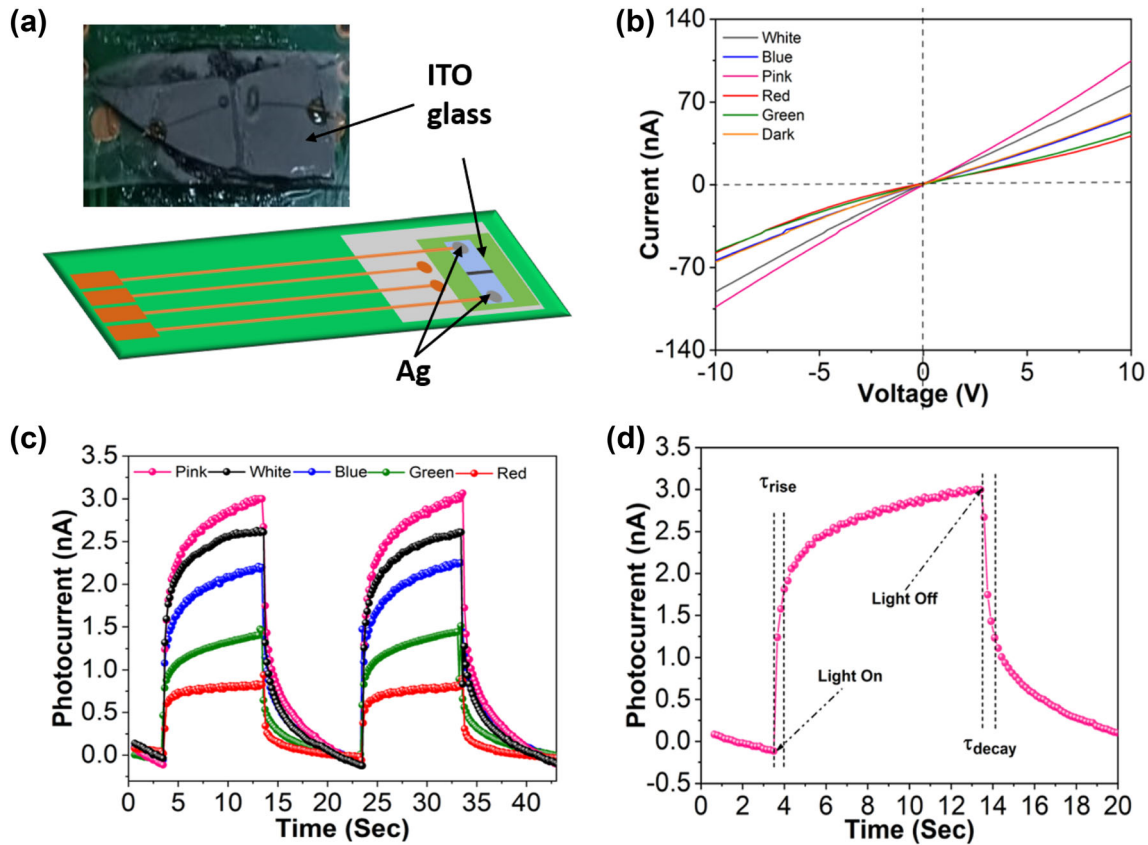


Fig. 4 **a** Schematic diagram of ITO/WSe₂ nanosheet-based photodetector, **b** I–V characteristics, and **c** pulse photoresponse under the illumination of different monochromatic and polychromatic wavelength sources with 40 mW/cm² power

d Magnified image of the single pulse based on ITO/WSe₂ nanosheets photodetector under pink (polychromatic) source

Table 1 Typical detector parameters of WSe₂ nanosheets photodetector device

Material	Sources	Photocurrent (nA)	Responsivity (μA/W)	Detectivity × 10 ⁸ (Jones)
WSe ₂	Pink (Visible)	2.93	3.65	1.08
	White (Visible)	2.50	3.11	0.68
	485 nm (Blue)	2.10	2.63	0.67
	532 nm (Green)	1.40	1.75	0.50
	670 nm (Red)	0.75	0.94	0.27

photodetector has a good reproductiveness at 1.0 V external bias.

Besides, the quantitative analysis can be done on typical photodetector parameters, such as responsivity and detectivity. It can be calculated using the below equations [38].

$$R = \frac{I_{ph}}{PS} \text{ and } D = \frac{R_s S^{1/2}}{(2eI_{dark})^{1/2}},$$

where I_{ph} indicates the photocurrent, S is the illuminated area of the photodetector ($\sim 0.02\text{cm}^2$), P

indicates the illumination intensity, and e is the electronic charge (1.6×10^{-19} C). The calculated values of the detector parameters are shown in Table 1.

Among all monochromatic and polychromatic sources, superior photoresponse is observed under the pink light illumination. In the case of a monochromatic light source, the photodetection properties improve when the wavelength of the source is decreased. The response time period is an important factor in determining photodetection activity as well as the performance of the device.

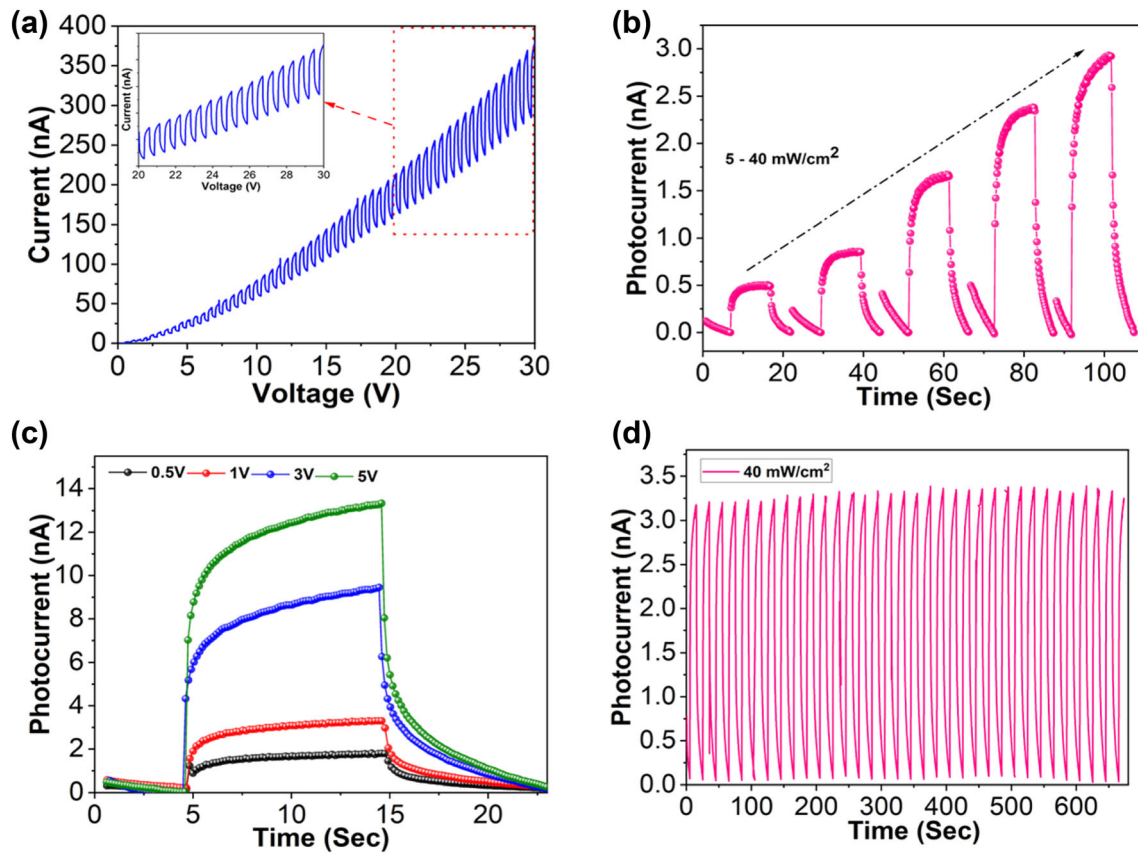


Fig. 5 **a** I–V curve of photodetector under periodic pink light source illumination with 40 mW/cm^2 power intensity, **b** pulse photoresponse of a device under pink (polychromatic) source illumination as a function of various power intensities, and **c** pulse

photoresponse of device under pink (polychromatic) source illumination as a function of various external bias voltages. **d** Stability curve at 1.0 V and 40 mW/cm^2 power intensity

Generally, the lifetime of the photogenerated charge carrier is the time needed to set up an equilibrium condition. The strong light–matter interaction in WSe_2 nanosheets is responsible for the increased photocurrent value [10, 39]. Two key factors to consider for high-performance switching devices are rise time (i.e., time required for current increasing up to 90%) and decay time (i.e., time required for current decreasing up to 10%) as shown in Fig. 4d. The values of the rise and decay time are 453 ms and 504 ms, respectively.

Furthermore, as presented in Fig. 5a, the device is tested for photoconduction at various external bias voltages. The I–V characteristic is examined by switching of light at periodic intervals. It is clear that as the external bias is increased, the photocurrent increases dramatically, implying that a high bias can improve the separation efficiency of charge carriers. The photocurrent is greatly increased up to 100 nA at 30 V, resulting in responsivity of $125.0 \mu\text{A/W}$ at a

pink light intensity of 40 mW/cm^2 . Then, the device was illuminated under a pink light source at various intensities ranging from 5 to 40 mW/cm^2 for 1.0 V external bias to examine the intensity-dependent photodetection properties. The photocurrent increases from 0.50 to 2.82 nA when the intensity of the light source is increased, as shown in Fig. 5b. Next, the applied external bias-dependent photodetection properties of the prepared device were investigated while being illuminated by a polychromatic pink light source with an intensity of 40 mW/cm^2 presented in Fig. 5c. When the external bias voltage was increased from 0.5 to 5.0 V, the photocurrent enhances from 1.63 to 10.22 nA. As shown in Fig. 5d, the device exhibits higher stability under a pink light source at 1.0 V external bias.

4 Conclusion

The bulk WSe₂ was grown successfully using the direct vapor transport technique. The WSe₂ nanosheets were produced by the liquid-phase exfoliation method (LPE). The mapping reveals the uniform distribution of all constituent elements, and the EDAX analysis indicates that no impurities are present in the grown material. The exfoliated WSe₂ has a hexagonal lattice structure. The micrograph shows the hexagonal shape of the grown crystal with a size of a few microns; whereas, the continuity of the film was confirmed by SEM image. The resonances corresponding to E_{2g} vibrational modes are seen in the Raman spectrum. The different lateral sizes of thin layers were observed in the HR-TEM image. The device showed excellent detection performance with photoresponsivity of 3.65 μA/W and photodetectivity of 1.08 × 10⁸ Jones under a pink light source for 1.0 V bias voltage. The maximum photoresponsivity of 125.0 μA/W is achieved for 30 V external bias.

Acknowledgements

Badal Chauhan would like to express their gratitude to the University Grants Commission of India (UGC) for providing a National fellowship under the OBC scheme. (NFO-2018-19- OBC-GUJ-71826).

Author contribution

BLC participated in the conceptualization, material preparation, data collection, investigation, analysis, and writing of the original draft. SAB participated in the investigation, data analysis, and methodology. SUG participated in the investigation and methodology. PMP participated in the data analysis and writing, reviewing, and editing of the manuscript. GKS acquired resources and assisted in project administration, writing, reviewing, and editing of the manuscript, and supervision. VMP assisted in project administration. VP acquired resources.

Data availability

The datasets generated during and analyzed during the current study are available from the corresponding author on reasonable request.

Declarations

Conflict of interest There are no conflicts to declare.

References

1. P.K. Kashyap, A. Kumar, R. Srivastava, S. Gupta, B.K. Gupta, *ChemNanoMat* **7**, 328 (2021)
2. S.U. Gupta, A.G. Dalvaniya, N.F. Patel, S.A. Bhakhar, S. Nair, J. Joy, K.D. Patel, G.K. Solanki, V.M. Pathak, N.N. Som, P.K. Jha, D.K. Panda, *A.C.S. Appl. Electron. Mater.* **3**, 4859 (2021)
3. F. Xia, H. Wang, Y. Jia, *Nat. Commun.* **5**, 1 (2014)
4. J. Xue, J. Sanchez-Yamagishi, D. Bulmash, P. Jacquod, A. Deshpande, K. Watanabe, T. Taniguchi, P. Jarillo-Herrero, B.J. Leroy, *Nat. Mater.* **10**, 282 (2011)
5. N. Alem, R. Erni, C. Kisielowski, M.D. Rossell, W. Gannett, A. Zettl, *Phys. Rev. B Condens. Matter Mater. Phys.* **80**, 1 (2009)
6. M. Chhowalla, H.S. Shin, G. Eda, L.J. Li, K.P. Loh, H. Zhang, *Nat. Chem.* **5**, 263 (2013)
7. A.M. Jones, H. Yu, J.S. Ross, P. Klement, N.J. Ghimire, J. Yan, D.G. Mandrus, W. Yao, X. Xu, *Nat. Phys.* **10**, 130 (2014)
8. P. Pataniya, G.K. Solanki, C.K. Zankat, M. Tannarana, C.K. Sumesh, K.D. Patel, V.M. Pathak, *Pramana - J. Phys.* **91**, 1 (2018)
9. K.F. Mak, C. Lee, J. Hone, J. Shan, T.F. Heinz, *Phys. Rev. Lett.* **105**, 2 (2010)
10. L. Britnell, R.M. Ribeiro, A. Eckmann, R. Jalil, B.D. Belle, A. Mishchenko, Y. Kim, R.V. Gorbachev, T. Georgiou, S.V. Morozov, N. Grigorenko, A.K. Geim, C. Casiraghi, H.C. Neto, K.S. Novoselov, *Science* **340**, 1311 (2013)
11. A. Splendiani, L. Sun, Y. Zhang, T. Li, J. Kim, C.Y. Chim, G. Galli, F. Wang, *Nano Lett.* **10**, 1271 (2010)
12. C. Berthier, Y. Chabre, M. Minier, *Solid State Commun.* **28**, 327 (1978)
13. J. Dai, M. Li, X.C. Zeng, *Wiley Interdiscip. Rev. Comput. Mol. Sci.* **6**, 211 (2016)
14. A. Patel, C. Limberkar, K. Patel, S. Bhakhar, K.D. Patel, G.K. Solanki, V.M. Pathak, *Sens. Actuators A Phys.* **331**, 112969 (2021)
15. K.Z. Du, X.Z. Wang, Y. Liu, P. Hu, M.I.B. Utama, C.K. Gan, Q. Xiong, C. Kloc, *ACS Nano* **10**, 1738 (2016)
16. S. Das, J.A. Robinson, M. Dubey, H. Terrones, M. Terrones, *Annu. Rev. Mater. Res.* **45**, 1 (2015)
17. S.J. An, Y.H. Kim, C. Lee, D.Y. Park, M.S. Jeong, *Sci. Rep.* **8**, 1 (2018)

18. Y. Gong, S. Lei, G. Ye, B. Li, Y. He, K. Keyshar, X. Zhang, Q. Wang, J. Lou, Z. Liu, R. Vajtai, W. Zhou, P.M. Ajayan, *Nano Lett.* **15**, 6135 (2015)
19. Q.D. Truong, M. Kempaiah Devaraju, Y. Nakayasu, N. Tamura, Y. Sasaki, T. Tomai, I. Honma, *ACS Omega* **2**, 2360 (2017)
20. H. Li, G. Lu, Y. Wang, Z. Yin, C. Cong, Q. He, L. Wang, F. Ding, T. Yu, H. Zhang, *Small* **9**, 1974 (2013)
21. X. Yu, M.S. Prévot, N. Guijarro, K. Sivula, *Nat. Commun.* **6**, 1 (2015)
22. H. Yuan, X. Liu, L. Ma, P. Gong, Z. Yang, H. Wang, J. Wang, S. Yang, *RSC Adv.* **6**, 82763 (2016)
23. R.C. RuiZhang, Daniel Drysdale, Vasileios kaoutsos. *Adv. Funct. Mater.* **27**, 1702455 (2017)
24. A. Kuc, *Chem. Model.* **11**, 1 (2015)
25. P. Pataniya, G.K. Solanki, C.K. Zankat, M. Tannarana, K.D. Patel, V.M. Pathak, *J. Mater. Sci. Mater. Electron.* **30**, 3137 (2019)
26. Q.H. Wang, K. Kalantar-Zadeh, A. Kis, J.N. Coleman, M.S. Strano, *Nat. Nanotechnol.* **7**, 699 (2012)
27. L. Li, Z. Chen, Y. Hu, X. Wang, T. Zhang, W. Chen, Q. Wang, *J. Am. Chem. Soc.* **135**, 1213 (2013)
28. A. Patel, P. Pataniya, S. Narayan, C.K. Sumesh, V.M. Pathak, G.K. Solanki, K.D. Patel, P.K. Jha, *Mater. Sci. Semicond. Process.* **81**, 108 (2018)
29. P.M. Pataniya, V. Patel, C.K. Sumesh, *Nanotechnology* **32**, 1 (2021)
30. S.A. Bhakhar, P.M. Pataniya, M. Tannarana, G.K. Solanki, V.M. Pathak, *Opt. Mater.* **125**, 112097 (2022)
31. M. Patel, P.M. Pataniya, D.J. Late, C.K. Sumesh, *Appl. Surf. Sci.* **538**, 148121 (2021)
32. D.L. Duong, S.J. Yun, Y.H. Lee, *ACS Nano* **11**, 11803 (2017)
33. R.P. Patel, P.M. Pataniya, M. Patel, C.K. Sumesh, *Nanotechnology* **32**, 5205202 (2021)
34. X.F. Zhang, M. Kobayashi, *Mater. Sci.* **4**, 1 (2017)
35. P. Pataniya, C.K. Zankat, M. Tannarana, C.K. Sumesh, S. Narayan, G.K. Solanki, K.D. Patel, V.M. Pathak, P.K. Jha, *A.C.S. Appl. Nano Mater.* **2**, 2758 (2019)
36. P.M. Pataniya, C.K. Sumesh, *ACS Appl. Energy Mater.* **4**(5), 4815 (2021)
37. P.M. Pataniya, C.K. Sumesh, *Synth. Met.* **265**, 116400 (2020)
38. S.U. Gupta, A.G. Dalvaniya, C. Limberkar, K.D. Patel, G.K. Solanki, V.M. Pathak, P.M. Pataniya, C.K. Sumesh, N.N. Som, P.K. Jha, V. Patel, *J. Non. Cryst. Solids* **578**, 121353 (2022)
39. L. Tao, Z. Chen, Z. Li, J. Wang, X. Xu, J. Xu, *InfoMat* **3**, 36 (2021)

Publisher's Note Springer Nature remains neutral with regard to jurisdictional claims in published maps and institutional affiliations.